Spectrochimica Acta Part A 79 (2011) 1240–1246

Contents lists available at ScienceDirect

Spectrochimica Acta Part A: Molecular and Biomolecular Spectroscopy

journal homepage: www.elsevier.com/locate/saa

Spectrofluorometric studies on the binding interaction of bioactive imidazole with bovine serum albumin: A DFT based ESIPT process

Jayaraman Jayabharathi*, Venugopal Thanikachalam, Kanagarathinam Saravanan, Marimuthu Venkatesh Perumal

Department of Chemistry, Annamalai University, Annamalainagar 608 002, Tamil Nadu, India

ARTICLE INFO

Article history:
Received 7 March 2011
Received in revised form 26 March 2011
Accepted 15 April 2011

Keywords:
Bioactive imidazole
ESIPT
PES
FRET
Binding distance
Binding constant

ABSTRACT

Bioactive imidazole derivatives were synthesized and characterized by NMR spectra, mass and CHN analysis. An excited state intramolecular proton transfer (ESIPT) process in hydroxy imidazole has been studied using emission spectroscopy. In hydrocarbon solvent, the tautomer emission predominates over the normal emission and in alcoholic solvent like ethanol; a dramatic enhancement of normal emission is observed which was due to increased solvation. DFT calculation on energy, charge distribution of the rotamers in the ground and excited states of the imidazole derivative were performed and discussed. PES calculation indicates that the energy barrier for the interconversion of two rotamers is too high in the excited state than in the ground state. The interaction between bioactive imidazole derivative and bovine serum albumin (BSA) was investigated.

1. Introduction

Bio-active imidazole derivatives attracted considerable attention because of their unique optical properties [1,2] and the imidazole nucleus forms the main structure of human organisms, i.e., the amino acid histidine, Vitamin B_{12}, a component of DNA base structure and also have analytical applications utilizing their fluorescence and chemiluminescence properties [3]. Excited state intramolecular proton transfer (ESIPT) phenomena have been investigated [4–8] in the past decades due to the practical applications of ESIPT exhibiting molecules as laser dyes [4], photo stabilizers [5], fluorescent probes in biology [6] and light-emitting materials for electroluminescent devices [7–9]. ESIPT occurs in aromatic molecules having a phenolic hydroxy group with an intramolecular hydrogen bond to the nearby hetero atom of the same chromophore.

Serum albumins are the most abundant proteins in plasma [10,11], among the serum albumins, BSA has a wide range of physiological functions involving the binding, transport and delivery of fatty acids, porphyrins, steroids, etc. Steady state and time-resolved fluorescence spectroscopy are used for analyzing the binding properties of BSA and drugs and also to study the structural information of protein cavities [12–14]. Fluorescence quenching is an important method to study the interaction of substances with protein because of its accuracy, sensitivity, rapidity and convenience of usage.

In the present paper, we will focus the light on the photophysical studies of 2-aryl imidazole derivatives (**1**–**6**), ESIPT process of hydroxy imidazole, density functional theory (DFT) calculation on energy, dipole moment and PES studies of various rotamers. We also exploited the detailed investigation of BSA–imidazole association (binding parameters and the effect of imidazole on the protein conformation) using fluorescence and UV–vis absorption studies.

2. Experimental

2.1. Materials and methods

Butane-2,3-dione (Sigma–Aldrich Ltd.), 4-fluoro benzaldehyde (S.D. fine.), 4-fluoro salicylaldehyde, 4-fluoro-2-methoxy benzaldehyde, 3-methyl aniline, 2,5-dimethyl aniline and all other reagents used without further purification. Bovine serum albumin (BSA) was obtained from Sigma–Aldrich Company, Bangalore. All BSA solution was prepared in the Tris–HCl buffer solution (0.05 mol L^{-1} Tris, 0.15 mol L^{-1} NaCl, pH 7.4) and was kept in the dark at 303 K. Tris base (2-amino-2-(hydroxymethyl)-1,3-propanediol) had a purity of not less than 99.5% and NaCl, HCl and other starting materials were all of analytical purity and doubly distilled water was used throughout.

* Corresponding author. Tel.: +91 9443940735.
E-mail address: jtchalam2005@yahoo.co.in (J. Jayabharathi).

1386-1425/$ – see front matter © 2011 Elsevier B.V. All rights reserved.
doi:10.1016/j.saa.2011.04.049

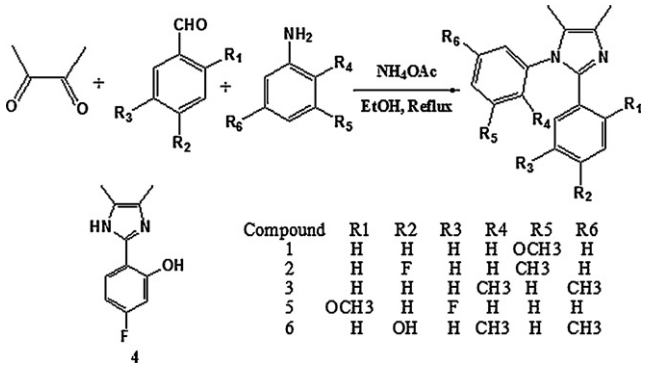

Compound	R1	R2	R3	R4	R5	R6
1	H	H	H	H	OCH3	H
2	H	F	H	H	CH3	H
3	H	H	H	CH3	H	CH3
5	OCH3	H	F	H	H	H
6	H	OH	H	CH3	H	CH3

Scheme 1. Synthesis of imidazole (**1**–**6**).

2.2. Optical measurements and composition analysis

NMR spectra were recorded on a Bruker 400 MHz. The UV–vis spectra and photoluminescence (PL) spectra were measured on UV–vis spectrophotometer (Perkin Elmer, Lambda 35) and fluorescence spectrometer (Perkin Elmer LS55), corrected for background due to solvent absorption. MS spectra were recorded on a Varian Saturn 2200 GCMS spectrometer. The quantum yield (Φ_p), radiative (k_r) and non-radiative (k_{nr}) deactivation pathways are calculated to be: $\Phi_{unk} = \Phi_{std}(I_{unk}/I_{std})(A_{std}/A_{unk})(\eta_{unk}/\eta_{std})^2$, where Φ_{unk}, Φ_{std}, I_{unk}, I_{std}, A_{unk}, Φ_{unk} and Φ_{std} are the fluorescence quantum yields, the integration of the emission intensities, the absorbances at the excitation wavelength and the refractive indexes of the corresponding solution of the 2-aryl imidazole derivatives (**1**–**6**) and the standard, respectively.

2.3. Computational details

Quantum mechanical calculations were carried out using Gaussian-03 program [15]. As the first step of our DFT calculation, the geometry taken from the starting structure was optimized.

2.4. General procedure for the synthesis of 2-aryl imidazole derivatives (*1*–*6*)

The experimental procedure was used as the same as described in our recent papers [16–24]. The 2-aryl imidazole derivatives (**1**–**6**) were synthesized from an unusual four components assembling of butane-2,3-dione, ammonium acetate, substituted anilines and substituted benzaldehydes (Scheme 1).

2.4.1. 4,5-Dimethyl-2-phenyl-1-m-tolyl-1H-imidazole (*1*)

Yield: 53%. ^{1}H NMR (400 MHz, $CDCl_3$): δ 2.00 (s, 3H), 2.28 (s, 3H), 2.36 (s, 3H), 6.97 (d, 2H), 7.18 (m, 4H), 7.23 (d, 1H), 7.33 (m, 2H). ^{13}C NMR (100 MHz, $CDCl_3$): δ 9.57, 12.75, 21.28, 125.00, 127.94, 128.40, 129.20, 130.93, 133.48, 137.94, 139.55, 145.06. Anal. calcd. for $C_{18}H_{18}N_2$: C, 82.41; H, 6.92; N, 10.68. Found: C, 82.22; H, 6.74; N, 10.46. MS: *m*/*z* 262.20, calcd. 262.15.

2.4.2. 2-(4-Fluorophenyl)-4,5-dimethyl-1-m-tolyl-1H-imidazole (*2*)

Yield: 55%. ^{1}H NMR (400 MHz, $CDCl_3$): δ 2.00 (s, 3H), 2.27 (s, 3H), 2.36 (s, 3H), 6.86 (s, 2H), 6.94 (s, 1H), 6.95 (s, 1H), 7.22 (d, 1H), 7.29 (m, 3H). ^{13}C NMR (100 MHz, $CDCl_3$): δ 9.53, 12.69, 21.26, 114.86, 115.08, 124.94, 125.34, 127.16, 128.35, 129.31, 129.81, 133.44, 137.73, 139.69, 144.19, 160.99, 163.45. Anal. calcd. for $C_{18}H_{17}N_2F$: C, 76.12; H, 6.11; N, 9.99. Found: C, 76.06; H, 5.96; N, 9.83. MS: *m*/*z* 281.30, calcd. 280.14.

2.4.3. 4,5-Dimethyl-1-(2,5-dimethylphenyl)-2-phenyl-1H-imidazole (*3*)

Yield: 47%. ^{1}H NMR (400 MHz, $CDCl_3$): δ 1.85 (s, 3H), 1.90 (s, 3H), 2.29 (s, 3H), 2.34 (s, 3H), 7.00 (s, 1H), 7.15 (m, 5H), 7.36 (m, 2H). ^{13}C NMR (100 MHz, $CDCl_3$): δ 9.10, 12.79, 16.84, 20.79, 124.94, 126.99, 127.45, 128.01, 129.81, 131.08, 132.76, 133.54, 136.90, 144.49, 160.94, 163.01. Anal. calcd. for $C_{19}H_{20}N_2$: C, 82.57; H, 7.29; N, 10.14. Found: C, 82.01; H, 6.98; N, 9.86. MS: *m*/*z* 276.30, calcd. 276.16.

2.4.4. 2-(4,5-Dimethyl-1H-imidazol-2-yl) 5-fluorophenol (*4*)

Yield: 44%. Anal. calcd. for $C_{11}H_{11}N_2OF$: C, 64.07; H, 5.38; N, 13.58. Found: C, 64.82; H, 5.92; N, 14.04. ^{1}H NMR (400 MHz, $CDCl_3$): δ 2.27 (s, 3H), 2.30 (s, 3H), 6.80–7.14 (aromatic protons), 10.30 (s, 1H), 12.20 (s, 1H). ^{13}C (100 MHz, $CDCl_3$): δ 9.42, 12.36, 116.40, 121.00, 127.23, 130.53, 146.08, 148.21, 154.30. MS: *m*/*z* 206.5, calcd. 206.22.

2.4.5. 2-(5-Fluoro-2-methoxyphenyl)-4,5-dimethyl-1-phenyl-1H-imidazole (*5*)

Yield: 47%. Anal. calcd. for $C_{18}H_{17}N_2OF$: C, 72.95; H, 5.78; N, 9.45. Found: C, 73.10; H, 5.97; N, 9.89. ^{1}H NMR (400 MHz, $CDCl_3$): δ 2.01 (s, 3H), 2.23 (s, 3H), 3.80 (s, 3H), 6.78–7.45 (aromatic protons), ^{13}C (100 MHz, $CDCl_3$): δ 9.43, 12.71, 55.28, 116.20, 118.00, 121.00, 127.23, 130.00, 134.48, 137.90, 144.31, 155.28. MS: *m*/*z* 296.03, calcd 296.34.

2.4.6. 4-(4,5-Dimethyl-1-(2,5-dimethylphenyl)-1H-imidazol-2-yl)phenol (*6*)

Yield: 49%. ^{1}H NMR (400 MHz, $CDCl_3$): δ 1.84 (s, 3H), 1.89 (s, 3H), 2.28 (s, 3H), 2.35 (s, 3H), 4.6 (s, 1H) 6.85 (m, 2H), 6.97 (s, 1H), 7.17 (d, 2H), 7.33 (m, 2H).^{13}C NMR (100 MHz, $CDCl_3$): δ 9.12, 12.83, 16.87, 20.85, 115.19, 124.97, 127.46, 128.92, 130.00 133.99, 136.98, 143.74, 161.01, 163.48. Anal. calcd. for $C_{19}H_{20}N_2O$: C, 77.52; H, 6.51; N, 9.52. Found: C, 77.01; H, 6.02; N, 9.21. MS: 292.16, calcd. 292.00.

2.5. Principles of fluorescence quenching

Fluorescence quenching [25] is described by the Stern–Volmer equation:

$$\frac{F_0}{F} = 1 + K_q\tau_0[Q] = 1 + K_{SV}[Q] \quad (1)$$

where F_0 and F are the fluorescence intensities before and after the addition of the quencher, respectively. K_q, K_{SV}, τ_0 and [Q] are the quenching rate constant of the bimolecular, the Stern–Volmer dynamic quenching constant, the average lifetime of the bimolecular without quencher ($\tau_0 = 10^{-8}$ s) and the concentration of the quencher, respectively. Obviously, $K_q = K_{SV}\tau_0$, hence, Eq. (1) was applied to determine K_{SV} by linear regression of a plot of F_0/F versus [Q].

2.6. Calculation of binding parameters

Apparent binding constant k_A and binding sites n [26] can be obtained from

$$\frac{\log(F_0 - F)}{F} = \log K_A + n \log[Q] \quad (2)$$

where F_0 and F are the fluorescence intensities before and after the addition of the quencher, [Q] is the total quencher concentration. By the plot of $\log(F_0 - F)/F$ versus log[Q], the number of binding sites n and binding constant K_A can be obtained.

Table 1
Absorption and photoluminescence spectral data of **1**–**6** in various solvents.

Solvent	Absorption[a] (λ, nm) (log ε)						Emission[b] (λ, nm)					
	1	2	3	4	5	6	1	2	3	4	5	6
1,4-Dioxane	274.0 (3.20)	276.0 (4.07)	274.0 (4.11)	276 (4.08)	278 (4.20)	275.0 (4.09)	360	363	362	365, 400 (sh)	360	362
Benzene	277.5 (3.83)	280.0 (3.88)	279.0 (3.94)	277 (3.98)	280 (4.07)	278.0 (4.03)	363	370	368	367	362	366
Chloroform	283.0 (4.06)	285.0 (4.48)	281.0 (4.50)	280 (4.18)	281 (4.31)	287.0 (4.30)	371	372	371	372	365	374
Ethyl acetate	284.0 (4.26)	288.0 (4.24)	284.0 (4.28)	282 (4.33)	282 (4.25)	290.0 (4.03)	378	377	375	376	366	377
Dichloromethane	286.5 (4.33)	290.0 (4.16)	288 (4.28)	286 (4.37)	285 (4.29)	292.0 (4.22)	386	381	384	380	368	384
Ethanol	288.0 (3.89)	291.0 (3.93)	293.0 (4.17)	290 (3.74)	291 (3.88)	295.0 (4.11)	391	383	388	388	370	385
Methanol	291.0 (4.07)	293.0 (4.07)	297.0 (4.26)	298 (4.11)	297 (4.32)	299.0 (4.04)	398	388	393	392	382	388
Acetonitrile	296.0 (4.17)	297.0 (4.17)	301.5 (3.07)	302 (4.13)	303 (4.31)	303.0 (4.09)	406	399	401	403	390	397

[a] UV–vis absorption measured in solution concentration = 1×10^{-5} M.
[b] Photoluminescence measured in solution concentration = 1×10^{-4} M.

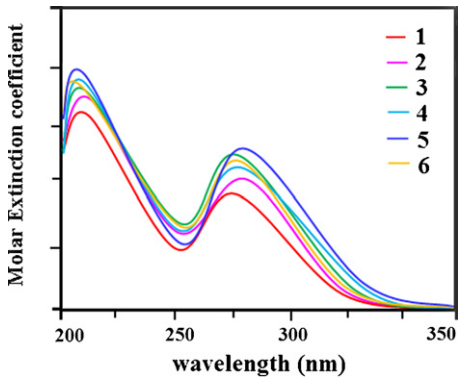

Fig. 1. Excitation spectra of 2-aryl imidazole derivatives **1**–**6** in ethanol.

3. Results and discussion

All 2-aryl imidazole derivatives (**1**–**6**) fluoresce strongly in solutions at room temperature. Their luminescence excitation spectra (Fig. 1) are in coincide with their absorption spectra and differ from their emission spectra (Fig. 2), therefore, the fluorescence of the 2-aryl imidazole derivatives (**1**–**6**) was taken for discussion (Table 1).

It may be suggested that in aprotic solvents, the hydroxy 2-aryl imidazole (**4**) exists as two different intramolecular hydrogen bonded isomers I and II (Fig. S1). Excitation of the isomer II should lead to the formation of the keto-isomer III due to ESIPT (Fig. S1), while excitation of the isomer I must yield the normal emission. But, we found out that the fluorescence spectra of **4** in dioxane contain an abnormal Stokes-shifted emission band and one small shoulder peak at higher wavelength which reveal that only the isomer II is stable under these conditions. Stokes shift is important for a fluorescent sensor, the higher Stokes shift value supplies very low background signals and resultantly allows the usage of the material in construction of a fluorescence sensor [27].

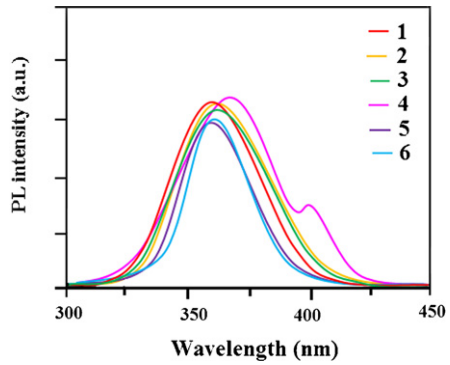

Fig. 2. Emission spectra of 2-aryl imidazole derivatives **1**–**6** in ethanol.

However, in the case of hydroxyl solvent (EtOH), a short wavelength emission band appears for **4** which is absent in the fluorescence spectra of **1**–**3**, **5** and **6** (Fig. 2). This result corresponds to the data obtained earlier [27,28] for compounds demonstrating ESIPT and can be explained by the presence of intermolecular hydrogen bonding with solvent molecule leading to the stabilization of solvated isomer IV in which ESIPT is impossible.

For better understanding the ESIPT mechanism in **4**, we performed DFT calculation of electron density for the keto and enol isomers of **4** in the ground and the excited states (Table 2) which reveal, excitation of enol isomer leads to an increase in electron density at N(5) atom and decrease at oxygen atom resulting in ESIPT and formation of the excited keto isomer in excited state, excited keto isomer emits luminescence and returns to the ground state keto form, which is characterized by a large positive charge at N(5) atom and negative charge at oxygen atom. As a result, a reverse process occurs in the ground state keto isomer producing an initial molecule in enol form.

3.1. Driving force for ESIPT process

The existence of intramolecular hydrogen bond in hydroxy imidazole **4** is confirmed by the presence of the singlet at 10.30 ppm in the ^{1}H NMR spectra which is a typical signal for hydrogen bonded hydrogen atom. In order to reveal the contribution of the intramolecular hydrogen bonding in the hydroxy imidazole **4** to their optical properties, the fluorescence spectra of compound **4** and its methoxy derivative **5** were measured in dioxane solvent under identical condition (Fig. 3). A dual fluorescence was detected for **4** with emission peak centered at 365 and 400 nm respectively. The emission peak at shorter wavelength at 365 nm is assigned to rotamer I and longer wavelength band at 400 nm is assigned to rotamer II whereas compound **5** exhibits emission peak only at 360 nm, absence of additional peak at longer wavelength confirms that absence of intramolecular hydrogen bond in **5** which further evident that intramolecular hydrogen bond is the essential driving force for ESIPT and the dual fluorescence behaviour of hydroxy imidazole **4**.

3.2. Potential energy curve

The ground and excited state geometries of the three rotamers, I, II, and III of **4** were optimized using the DFT/6-31G(d,p) and CIS

Table 2
Electron density of atoms N(5) and O for 4.

Atom	II	II*	III
N(5)	−0.398	−0.482	0.362
O	−0.581	−0.503	−0.786

* Excited state isomer II

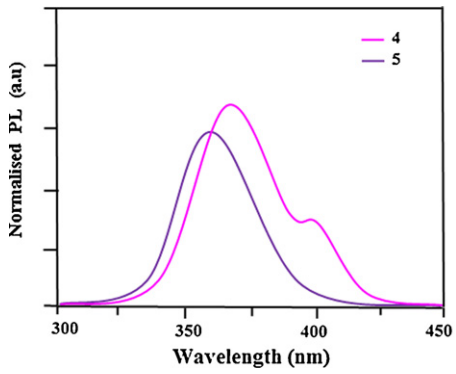

Fig. 3. Fluorescence spectra of **4** and **5** in dioxane.

Table 3
Relative energies (eV) and dipole moments (D) of 4 in the ground and excited state for rotamers I, II and III.

Rotamers	Ground state		Excited state	
	μ (D)	E (eV)[a]	E (eV)[a]	μ (D)
I	3.82	0.06 (0.00)	4.26 (3.62)	9.02
II	3.03	0.10 (0.06)	4.32 (3.96)	8.68
III	5.69	0.68 (0.42)	4.01 (3.36)	5.01

[a] Relative energies are calculated with respect to the ground state minimum energy form in ethanol. Values in the parenthesis are recorded in ethanol.

methods [28–30] respectively (Table 3). In the excited state the nitrogen atom becomes richer in electrons than the hydroxylic oxygen atom. This redistribution of the π-electron densities in the excited electronic state is the driving force for the intramolecular proton transfer from the hydroxylic group to the nitrogen atom. The potential energy (PE) curves (Fig. 4a and b) reveal that the energy barrier for the interconversion of isomers I and II of **4** in the ground state is 4.9 kcal/mol and 3.2 kcal/mol and in the excited state is 12.9 and 10.01 kcal/mol for isolated molecule and in ethanol, respectively. The barriers for interconversion in the excited state are much higher than that in the ground state (Table 3) and so the interconversion of isomers I and II is not possible in excited state.

3.3. Binding interaction of BSA with bioactive imidazole derivative

The interaction between bioactive imidazole derivative and bovine serum albumin (BSA) was investigated using fluorescence and UV–vis spectral studies and the fluorescence quenching of BSA by imidazole derivative was the result of the formation of BSA–imidazole complex. The binding site number (n) and apparent binding constant (K_A) were measured. The absorption spectra of BSA in the presence and absence of imidazole were different (Fig. 5). The absorption band of 210 nm of BSA is the characteristic of α-helix structure of BSA. The intensity of absorbance of BSA was decreased with increasing concentration of imidazole **6** and the peak was red shifted. The results indicated that there exists interaction between imidazole (**6**) and BSA results ground state complex was formed [31–33].

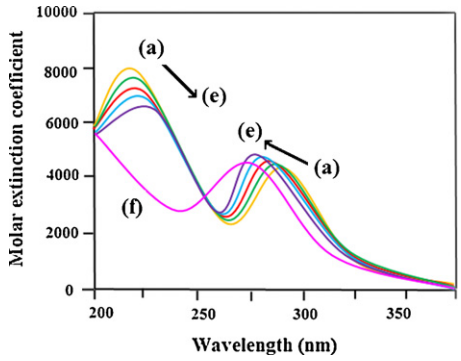

Fig. 5. Absorption spectra of BSA in the presence of imidazole (**6**) (a–e) and absence of imidazole (**6**) (f).

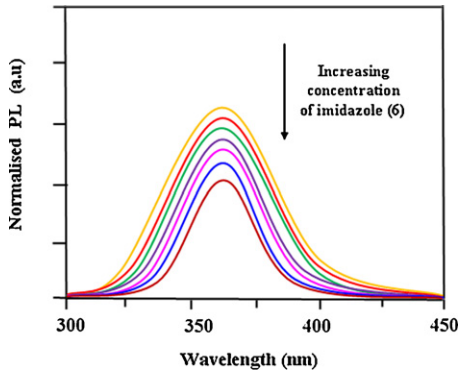

Fig. 6. Fluorescence quenching spectra of BSA at different concentrations of imidazole (**6**).

Fluorescence quenching spectra (Fig. 6) of solutions containing BSA fixed concentration and different concentrations of imidazole. It can be observed that the fluorescence intensity of BSA decreases regularly with the increase addition of imidazole (**6**) but there is no significant emission wavelength shift, suggest that imidazole (**6**) interact with BSA and quench its intrinsic fluorescence. A Forster type fluorescence resonance energy transfer (FRET) mechanism (Fig. 7) is involved in the quenching of *Trp* fluorescence by

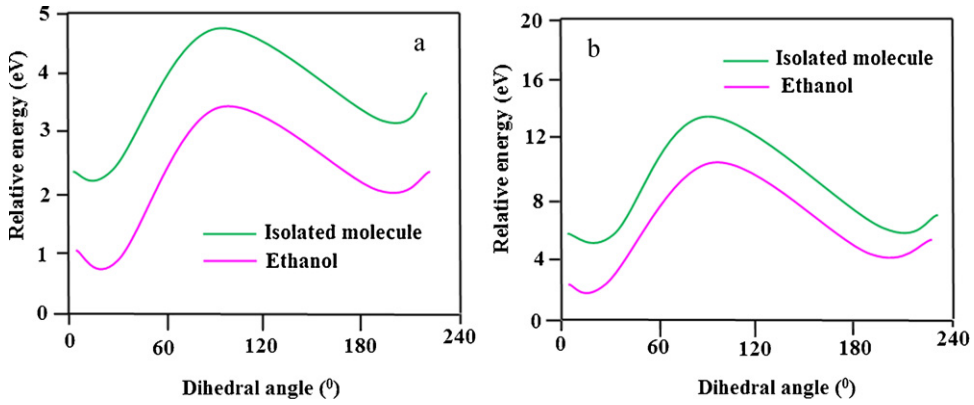

Fig. 4. (a) PES for the interconversion of the rotamers of **4** in the ground state. (b) PES for the interconversion of the rotamers of **4** in the excited state.

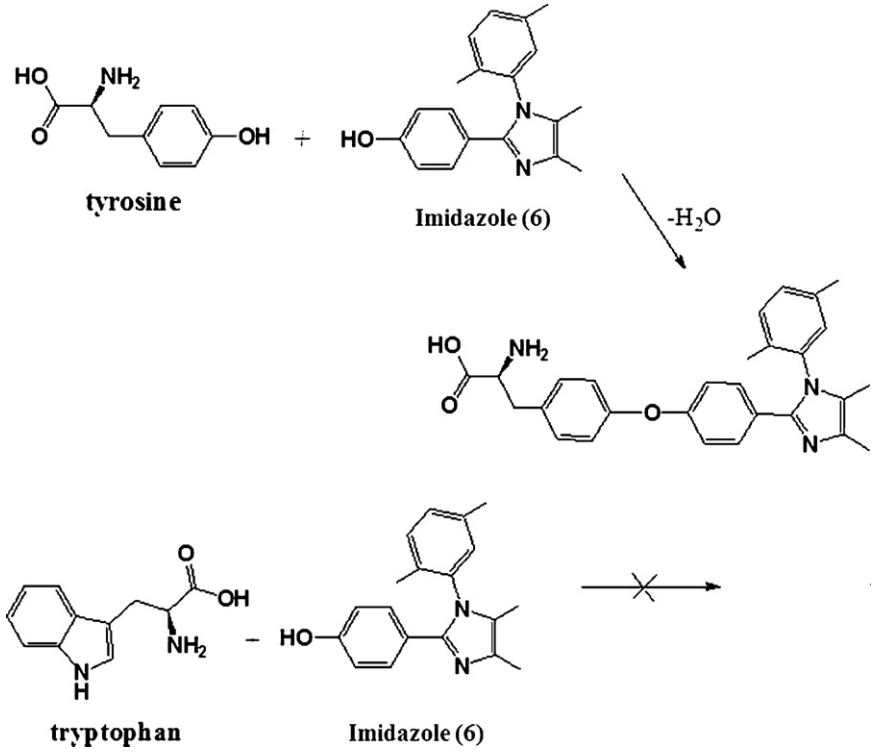

Scheme 2. Schematic representation of binding interaction of BSA with PPP.

imidazole **6** in BSA–imidazole (**6**) complex. This means that the possible quenching mechanism of fluorescence of BSA by imidazole is not initiated by dynamic collision but from the formation of the BSA–imidazole (**6**) complex (Scheme 2).

3.4. Fluorescence quenching mechanism

The quenching mechanism of imidazole (**6**) with BSA was probed using the Stern–Volmer equation [34]. Eq. (1) was applied to determine K_{SV} by linear regression from the Stern–Volmer plot of F_0/F against [imidazole] (Fig. 9). Dynamic and static quenching can be distinguished by the quenching constant K_q. According to the literature [35] for dynamic quenching, the maximum scatter collision quenching constant of various quenchers with the biopolymer is 2.0×10^{10} L mol^{-1} s^{-1} and the fluorescence lifetime of the biopolymers is 10^{-8} s [36]. From Fig. 8, the values of K_{SV} and K_q ($=K_{SV}/\tau_0$) was calculated. The values of K_q are larger

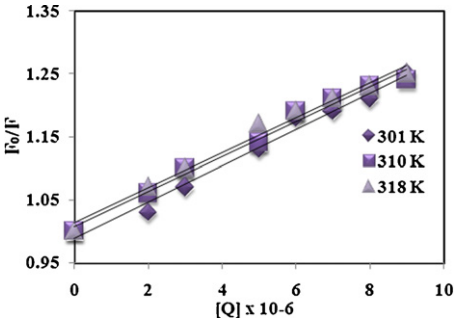

Fig. 8. Stern–Volmer plot of F_0/F against [imidazole].

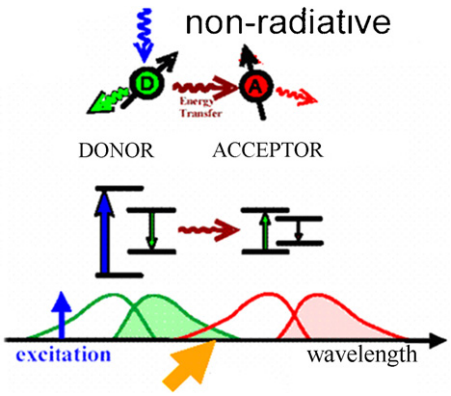

Fig. 7. Fluorescence resonance energy transfer (FRET) mechanism.

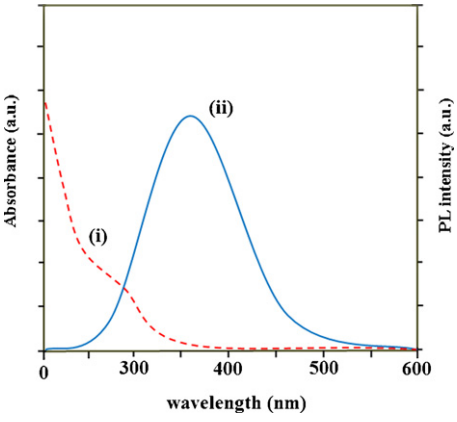

Fig. 9. Overlapping of fluorescence spectra of BSA with absorption spectra of PPP.

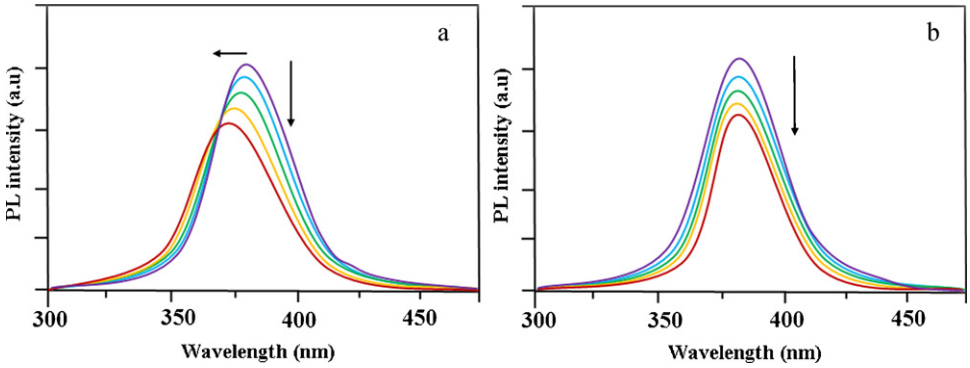

Fig. 10. Synchronous fluorescence spectra of BSA in the presence and absence of imidazole (a) at $\Delta\lambda = 15$ nm and (b) at $\Delta\lambda = 60$ nm.

than 2.0×10^{10} L mol^{-1} s^{-1}, which suggest that the fluorescence quenching is caused by a specific interaction between BSA and imidazole (**6**) and the quenching mechanism mainly arise from BSA–imidazole (**6**) complex formation (Fig. S2), while dynamic collision could be negligible in the concentration range studied [37]. The plot of $\log[(F_0 - F)/F]$ versus log[imidazole] binding constant K_A as 2.52×10^4 M^{-1} (301 K) and binding sites "*n*" (1.14) (301 K) of imidazole with BSA from the intercept and slope.

3.5. Energy transfer from BSA to imidazole derivative

The distance between the buried *Trp*-212 and the interacted imidazole was estimated by Forster's non-radiative energy transfer theory and the overlap fluorescence spectra of imidazole and the UV–vis absorption spectra of BSA was shown in Fig. 9. According to Forster's non-radiative energy transfer theory, the energy transfer efficiency (E) is defined as the following equations:

$$E = 1 - \frac{F}{F_0} = \frac{R_0^6}{R_0^6 + r_0^6} \quad (3)$$

$$R_0^6 \ (\text{Å}^6) = 8.8 \times 10^{23}[k^2 n^{-4} \Phi_D J(\lambda)] \quad (4)$$

$$J(\lambda) = \int_0^\infty F_D(\lambda)\varepsilon_A(\lambda)\lambda^4 \, d\lambda \quad (5)$$

$F_D(\lambda)$ is the corrected fluorescence intensity of the donor at wavelength λ to $(\lambda + \Delta\lambda)$, with the total intensity normalized to unity and $\varepsilon_A(\lambda)$ is the molar extinction coefficient of the acceptor at wavelength λ. The Forster distance (R_0) has been calculated assuming random orientation of the donor and acceptor molecules. In the present case, $\kappa^2 = 2/3$, $n = 1.334$, $\Phi_D = 0.42$ and from the available data, it results that $J(\lambda) = 2.45 \times 10^{-15}$ cm^3 L mol^{-1}, $E = 0.34$, $R_0 = 1.92$ nm and $r = 2.2$ nm were calculated. The donor-to-acceptor distance is less than the 8 nm, and the long distance indicates that the quenching mechanism is a dynamic one, which is strong evidence for static quenching and energy could transfer from BSA to imidazole (**6**) [38].

3.6. Synchronous fluorescence spectroscopic studies of BSA

The synchronous fluorescence spectra [39–41] of BSA with various amounts of imidazole (**6**) were recorded at $\Delta\lambda = 15$ nm and $\Delta\lambda = 60$ nm (Fig. 10a and b), respectively. The emission wavelength of the tyrosine residues is blue-shifted (λ_{max} from 362 to 351 nm in Fig. 10a) with increasing concentration of imidazole. At the same time, the tryptophan fluorescence emission is decreased regularly, but no significant change in wavelength was observed. It suggests that the interaction of imidazole with BSA does not affect the conformation of tryptophan micro-region. The tyrosine fluorescence spectrum may represent that the conformation of BSA is somewhat changed, leading to the polarity around *Tyr* residues strengthened and the hydrophobicity weakened [42]. This is because tyrosine contains one aromatic hydroxyl group unlike tryptophan and tyrosine can undergo an excited state ionization, resulting in the loss of the proton on the aromatic hydroxyl group. The hydroxyl group can dissociate during the lifetime of its excited state, leading to quenching. Hence the aromatic hydroxyl group present in the tyrosine residues is responsible for the interaction of BSA with imidazole.

4. Conclusion

Tautomer emission dominates over normal emission in alcohol at room temperature for hydroxy imidazole. The DFT calculations indicate in the excited state, the nitrogen atom becomes richer in electrons than the hydroxylic oxygen atom. This redistribution of the π-electron densities in the excited electronic state is the driving force for the intramolecular proton transfer from the hydroxylic group to the nitrogen atom. PES calculation reveals that the barriers for interconversion in the excited state are much higher than that in the ground state. So, the interconversions of rotamers are not possible. The interaction between bioactive imidazole derivative and bovine serum albumin (BSA) was investigated. The possible quenching mechanism of fluorescence of BSA by imidazole is not initiated by dynamic collision but from the formation of the BSA–imidazole (**6**) complex.

Acknowledgments

One of the author Dr. J. Jayabharathi, associate professor of Chemistry, Annamalai University is thankful to Department of Science and Technology [No. SR/S1/IC-07/2007] and University Grants commission (F. No. 36-21/2008 (SR)) for providing fund to this research work.

Appendix A. Supplementary data

Supplementary data associated with this article can be found, in the online version, at doi:10.1016/j.saa.2011.04.049.

References

[1] W.S. Hung, J.T. Lin, C.H. Chien, Y.T. Tao, S.S. Sun, Y.S. Wen, Chem. Mater. 16 (2004) 2480–2488.
[2] K. Nakashima, Biomed. Chromatogr. 17 (2003) 83–85.
[3] A. Mallick, S.C. Bera, S. Maiti, N. Chattopadhya, Biophys. Chem. 112 (2004) 9–14.
[4] P.T. Chou, M.L. Martinez, J.H. Clements, J. Phys. Chem. 97 (1993) 2618–2622.
[5] L.F. Campo, F.S. Rodembusch, V. Stefani, J. Appl. Polym. Sci. 99 (2006) 2109–2116.
[6] Y. Wu, X. Peng, J. Fan, S. Gao, M. Tian, J. Zhao, S. Sun, J. Org. Chem. 72 (2007) 62–66.

[7] S. Park, O.H. Kwon, Y.S. Lee, D.J. Jang, S.Y. Park, J. Phys. Chem. A 111 (2007) 9649–9653.
[8] S. Park, J. Seo, S.H. Kim, S.Y. Park, Adv. Funct. Mater. 18 (2008) 726–731.
[9] K. Das, N. Sarkar, A.K. Ghosh, D. Majumdar, D.N. Nath, K. Bhattacharyya, J. Phys. Chem. 98 (1994) 9126–9132.
[10] D.D. Carter, J.X. Ho, Adv. Protein Chem. 45 (1994) 153–203.
[11] F. Moreno, M. Cortijo, J.G. Jimenez, Photochem. Photobiol. 70 (1999) 695–700.
[12] D. Gao, Y. Tian, F. Liang, D. Jin, Y. Chen, H. Zhang, A. Yu, J. Lumin. 127 (2007) 515–522.
[13] X.M. He, D.C. Carter, Nature 358 (1992) 209–215.
[14] R.D. Gray, S.D. Stroupe, J. Biochem. 253 (1978) 4370–4377.
[15] Guassian 03 program, Gaussian Inc., Wallingford, CT, 2004.
[16] J. Jayabharathi, V. Thanikachalam, K. Saravanan, N. Srinivasan, J. Fluoresc. (2010), doi:10.1007/s10895-010-0737-7.
[17] K. Saravanan, N. Srinivasan, K. Thanikachalam, J. Jayabharathi, J. Fluoresc. 21 (2010) 65–80.
[18] P. Gayathri, J. Jayabharathi, N. Srinivasan, A. Thiruvalluvar, R.J. Butcher, Acta Crystallogr. E 66 (2010) o1703.
[19] P. Gayathri, A. Thiruvalluvar, K. Saravanan, J. Jayabharathi, R.J. Butcher, Acta Crystallogr. E 66 (2010) o2219.
[20] P. Gayathri, J. Jayabharathi, N. Srinivasan, A. Thiruvalluvar, R.J. Butcher, Acta Crystallogr. E 66 (2010) o2519.
[21] J. Jayabharathi, V. Thanikachalam, N. Srinivasan, K. Saravanan, J. Fluoresc. (2010), doi:10.1007/s10895-010-0747-5.
[22] J. Jayabharathi, V. Thanikachalam, K. Saravanan, N. Srinivasan, M. Venkatesh Perumal, Spectrochim. Acta A 78 (2010) 794–802.
[23] J. Jayabharathi, V. Thanikachalam, K. Jayamoorthy, M. Venkatesh Perumal, Spectrochim. Acta A (2010), doi:10.1016/j.saa.2010.12.027.
[24] J. Jayabharathi, V. Thanikachalam, K. Saravanan, J. Photochem. Photobiol. A Chem. 208 (2009) 13–20.
[25] Y.J. Hu, Y. Liu, L.X. Zhang, J. Mol. Struct. 750 (2005) 174–178.
[26] M. Jiang, M.X. Xie, D. Zheng, Y. Liu, X.Y. Li, X. Chen, J. Mol. Struct. 692 (2004) 71–80.
[27] M.Y. Ismet Kaya, J. Fluoresc., in press.
[28] P.F. Barbara, P.K. Walsh, L.E. Brus, J. Phys. Chem. 93 (1989) 29–34.
[29] G.J. Woolfe, M. Melzig, S. Schneider, F. Dörr, Chem. Phys. 77 (1983) 213–221.
[30] A.L. Sobolewski, Chem. Phys. Lett. 211 (1993) 293–299.
[31] K. Fukui, T. Yonezawa, H. Shingu, J. Chem. Phys. 20 (1952) 722–725.
[32] Q. Sun, Z. Li, X. Zeng, M. Ge, D. Wang, J. Mol. Struct. (Theochem.) 724 (2005) 167–172.
[33] W. He, Y. Li, C. Xue, Z.D. Hu, X.G. Chen, Bioorg. Med. Chem. 13 (2005) 1837–1844.
[34] J.R. Lakowicz, Principles of Fluorescence Spectroscopy, 3rd ed., Springer Publisher, New York, 2006.
[35] H. Cao, D. Wu, H. Wang, M. Xu, Spectrochim. Acta A 73 (2009) 972–975.
[36] T.G. Dewey, Biophysical and Biochemical Aspects of Fluorescence Spectroscopy, Plenum Press, New York, 1991, pp. 1–41.
[37] M.M. Yang, X.L. Xi, P. Yang, Chin. J. Chem. 24 (2006) 642–648.
[38] J. Jayabharathi, V. Thanikachalam, M. Venkatesh Perumal, N. Srinivasan, Spectrochim. Acta A 79 (2011) 236–244.
[39] G.Z. Chen, X.Z. Huang, J.G. Xu, Z.Z. Zheng, Z.B. Wang, Methods of Fluorescence Analysis, 2nd ed., Science Press, Beijing, 1990.
[40] J.N. Miller, Proc. Anal. Div. Chem. Soc. 16 (1979) 203–208.
[41] J.H. Tang, F. Luan, X.G. Chen, Bioorg. Med. Chem. 14 (2006) 3210–3217.
[42] B. Klajnert, M. Bryszewska, Bioelectrochemistry 55 (2002) 33–35.